



**RESEARCH ARTICLE**

**COMPARISON of ANALYTICAL and FINITE ELEMENT SOLUTIONS of LOW VELOCITY IMPACT PROBLEM for SIMPLY SUPPORTED BEAM**

Yaşar ERBAŞ<sup>1</sup>, Bahadır ALYAVUZ<sup>2,\*</sup>

<sup>1</sup>Bartın University, Faculty of Engineering, Architecture and Design, Department of Civil Engineering, Bartın, [yerbas@bartin.edu.tr](mailto:yerbas@bartin.edu.tr), ORCID: 0000-0002-3475-9678

<sup>2</sup>Gazi University, Faculty of Engineering, Department of Civil Engineering, Ankara, [balyavuz@gazi.edu.tr](mailto:balyavuz@gazi.edu.tr), ORCID: 0000-0003-4643-4368

*Receive Date: 26.07.2022*

*Accepted Date: 09.11.2022*

**ABSTRACT**

The aim of this study is to compare the results obtained from analytical and finite element solutions of low velocity transverse impact problem of a sphere onto simply supported beam. Twelve models with various mass ratios were created by keeping the beam dimensions constant and changing the sphere radius. The effect of the element size in the finite element solution was analyzed with five separate meshes whose element size gradually decreases at the impact point. In the solutions, the deflections of the beam and the displacement of the sphere at the impact point were taken into account. To check the validity of the model, a comparison with an experimental study in the literature was also made. Comparisons show that the deflections obtained from the analytical solution are compatible with the finite element solution within the period of repetitive or continuous contact between the sphere and beam. Particularly, as the mass ratio defined for beam and sphere gets smaller, maximum deflection values obtained from analytical and finite elements become closer. For the cases including sub-impact, after the sphere leaves the beam there exist differences in the results mainly because of the sub-impacts.

**Keywords:** *Low velocity transverse impact, Analytical solution, Finite element analysis.*

**1. INTRODUCTION**

Research on the impact problem of beam-type structures helps to understand the behavior of this structural element and to make designs that consider dynamic effects. One of the fundamental problems frequently addressed is the impact of a spherical object in the transverse direction. An early work was done by Cox to find the deflection of a beam impacted by a ball in transverse direction [1]. The problem was considered by Timoshenko [2] in more detail with a theoretical work after the development of local contact deformations theory by Hertz [3].

A simple approach for an analytical solution to the problem considers the beam as a massless spring. It is indicated that significant difference between the results obtained with this approach and the experimental results were due to the absence inertial effects of the beam [4]. A procedure that considers the mass of the beam is a completely inelastic impact approach that takes into account that a fraction of the beam mass and the sphere have a common velocity immediately after the impact [4, 5]. In this case, the energy equations are written considering the mass of beam. In case the beam vibrations were considered, the time-varying impact force can be expressed as a nonlinear integral equation by considering displacements and Hertz contact law at the point of impact. This integral equation can be solved by various approximate methods to calculate the maximum contact force and contact duration in case of transverse impact on beam and plate type structures [6]. In these calculations, the operations are time consuming and the integral equation to calculate the impact force can be solved by simplification provided that the beam support type is not effective on the formation of the maximum impact load [7]. An adequate and fast approximate solution for determining the beam deflections as a function of time is the analytical approach that takes into account the free vibrations of the elastic beam where the contact force not need to be calculated [4]. This approach is summarized in the next section.

In addition to analytical methods, two or three-dimensional finite element (FE) models of structural elements are frequently used to investigate the impact behavior in more complex cases including concrete [8], reinforced concrete [9-12], composite [13, 14] beams and slabs. The formation of the impact requires determining partial or complete contact state of the two impacting bodies and their separation over time so that the problem is considered primarily as the contact-impact problem [15-17]. ABAQUS [18], a comprehensive and general-purpose finite element software, is one of the tools that enables such computational simulations for several decades [19-24].

The following studies can be included to evaluate relevant studies on the low velocity impact of a sphere striker on a flexible beam. Considering the impact duration, Pashah et al. proposed a simplified half space approximation to estimate this for elastic and elastic-plastic simply supported beams, and performed 3d finite element analysis in ABAQUS in order to consider the structural effects [25]. They also presented a spring-mass model to take into account the structural response in the simplified analytical approach and indicated the range at which it produced good results based on a period ratio. To obtain a faster solution compared to finite element analysis, Zhang et al. [26] proposed a hybrid numerical-analytical approach for a simply supported elastic-perfectly plastic beam. Among the works which interested in the path of the sphere after the impact, Seifried [27] conducted experimental and numerical research on aluminum beams and noted a chaotic behavior for the coefficient of restitution due to the sub-impacts. The sub-impact phenomenon, repeated contacts between striker and beam after initial contact, was initially mentioned by Timoshenko [2] and Arnold [28]. This was later investigated widely by Qi and Yin using steel beams, and they stated that these repeated contacts were affected by local deformations and global vibrations of the beam [29]. In addition, using LS-DYNA [30], they numerically simulated their experimental work and highlighted factors affecting the duration of repeated impacts and the conditions of the sub-impact formation [31].

In the following sections, the analytical formulation given by Goldsmith [4] for the beam deflections that occurred after the initial contact is summarized, the ABAQUS model for the finite element solution is explained and the results obtained from these two solutions are compared respectively.

## 2. ANALYTICAL a FINITE ELEMENT SOLUTIONS

If the mass of the beam is not negligible compared to the mass of the impacting object, the calculation should be made by taking into account the vibration and local deformation occurring in the beam [32]. Such an elastic impact problem has a more complex solution than the non-elastic impact problem where the beam mass can be neglected. Goldsmith [4], expressed the beam deflections as a series expression, starting from the governing differential equation of the forced vibration problem of the beam. Here, for a transverse impact of a rigid sphere of mass  $m_2$  onto a simply supported beam of length  $L$  and mass  $m_1$  with a velocity of  $v_2$  as shown in Fig. 1, the formulation of the equation of the deflections of the beam will be summarized [4]. The analytical model assumes a uniform Euler-Bernoulli beam and a sphere which is attached to the beam after the impact. Impact force is replaced by an initial condition for velocity immediately after the impact. In the analytical and finite element solutions, it is considered that the behavior is linearly elastic and the material is homogeneous and isotropic. No damping is taken into account unless it is specified as in section 2.3.

When one-dimensional transverse impact problem is to be solved based on the beam vibration problem, a solution can be obtained from the following forced vibration differential equation.

$$EI \frac{\partial^4 w}{\partial x^4} + \rho A \frac{\partial^2 w}{\partial t^2} = F \# \tag{1}$$

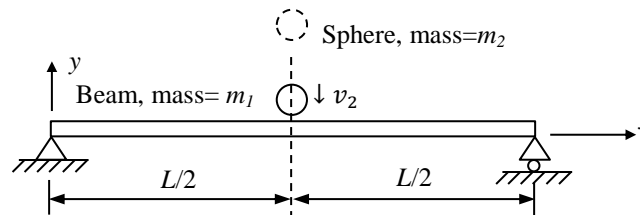


**Figure 1.** Properties of beam and sphere for transverse central impact.

where,  $w$  is the displacement of the beam in the transverse direction,  $F$  is a time-dependent force per unit length exerted by the sphere on the beam at contact point. Goldsmith [4] wrote the displacement of the beam as a series summation of the product of two position-dependent and time-dependent discrete functions in the analytical solution that considers vibration as follows,

$$w = \sum_{i=1}^{\infty} X_i(x) q_i(t) \# \tag{2}$$

This displacement function must satisfy the differential equation given in Eq. 1. At this point, Goldsmith [4] re-expressed the kinetic and potential energy functions of the beam using the

displacement in Eq. 2, and by writing these energy functions into the Lagrangian equation of motion, defined a function for  $q_i(t)$ .

This function, and therefore the displacement function, involves an unknown forcing function that occurs on the beam at the impact, which changes with time and must be calculated to fully express the displacement. In order to calculate this forcing function, an equation can be written by considering the displacement of the striker and the deflection of the beam at the impact point are equal. But, it is stated that this equation does not have a solution in a closed form and must be solved by a computational method.

Instead of solving the forced vibration problem to obtain an approximate analytical solution of the displacement function, Goldsmith [4] proposed a solution of the beam's free vibration associated with the impulse replaced by a suitable boundary condition. The transverse free vibration equation can be written by setting the forcing function  $F$  in Eq. 1 equal to zero. Writing Eq. 2 into the transverse free vibration equation yields,

$$EI \sum_{i=1}^{\infty} q_i \frac{\partial^4 X_i}{\partial x^4} + \rho A \sum_{i=1}^{\infty} X_i \frac{\partial^2 q_i}{\partial t^2} = 0 \# \quad (3)$$

Each term in the series summation must be equal to zero in order to satisfy the above equation, as follows,

$$a^4 q_i \frac{\partial^4 X_i}{\partial x^4} + X_i \frac{\partial^2 q_i}{\partial t^2} = 0 \# \quad (4)$$

where  $a^4 \equiv \frac{EI}{\rho A}$ . This partial differential equation can be solved by considering,

$$\frac{1}{X_i} \frac{\partial^4 X_i}{\partial x^4} = - \frac{1}{a^4 q_i} \frac{\partial^2 q_i}{\partial t^2} = \xi_i^4 \# \quad (5)$$

where  $\xi_i$  is an arbitrary constant and there are two separate differential equations. Solving these two differential equations for  $X_i$  and  $q_i$ , and by writing these two solutions into Eq. 2 yields,

$$w = \sum_{i=1}^{\infty} (A_i \sin \xi_i x + B_i \cos \xi_i x + C_i \sinh \xi_i x + D_i \cosh \xi_i x) (E_i \sin \omega_i t + F_i \cos \omega_i t) \# \quad (6)$$

where  $A_i$ ,  $B_i$ ,  $C_i$ , and  $D_i$  are constants to be determined from boundary conditions and  $E_i$ , and  $F_i$  are constants to be determined from initial conditions. For a simply supported beam, the boundary conditions are given by,

$$w(0, t) = 0; \quad \frac{\partial^2 w}{\partial x^2}(0, t) = 0; \quad \frac{\partial w}{\partial x}(\frac{L}{2}, t) = 0; \quad EI \frac{\partial^3 w}{\partial x^3}(\frac{L}{2}, t) = \frac{1}{2} m_2 \frac{\partial^3 w}{\partial t^3}(\frac{L}{2}, t) \# \quad (7)$$

where displacement, moment at the supports and slope at the mid-span are equal to zero, and shear at the contact point is equal the reversed effective force of the striker. Substitution of first three conditions into Eq.6 with  $w(x, 0) = 0$  yields the displacement function as,

$$w(x, t) = \sum_{i=1}^{\infty} \frac{1}{a^2 \xi_i^2} G_i X_i \sin \xi_i^2 a^2 t \quad \# \quad (8)$$

where  $G_i = a^2 \xi_i^2 E_i A_i \cos \frac{1}{2} \xi_i L$  is constant, and  $X_i = \frac{\sin \xi_i x}{\cos \frac{1}{2} \xi_i L} - \frac{\sinh \xi_i x}{\cosh \frac{1}{2} \xi_i L}$  is a function of  $x$ . Substitution Eq. 8 into the last condition in Eq.7 yields the following characteristic equation,

$$\phi_i (\tan \phi_i - \tanh \phi_i) = 2M \quad \# \quad (9)$$

where  $\phi_i = \frac{1}{2} \xi_i L$  and  $M = \frac{m_1}{m_2}$ . Solution of this equation gives  $\phi_i$  or its equivalent  $\xi_i$ .

In order to determine the unknown constant  $G_i$ , the displacement function needs be converted to include the impactor's speed at the time of impact. If the impactor transfers its velocity entirely to the infinitesimal part of the beam at the contact point, momentum of the impactor just before the impact,  $m_2 v_2$ , should be equal to the sum of the momentum of this part of the beam and the momentum of impactor just after the impact. At  $t = 0$ , this momentum equality is written as,

$$\int \frac{\partial w}{\partial t} \Big|_{(x,t=0)} d\bar{Q} = m_2 v_2 \quad \# \quad (10)$$

where  $\bar{Q}$  represents total mass of beam and impactor. The left hand side of this equation can also be written in terms of beam mass and impactor mass as,

$$2 \int_{x=0}^{\frac{L}{2}} \frac{\partial w}{\partial t} \left( \frac{m_1}{L} dx \right) + \frac{\partial w}{\partial t} m_2 \quad \# \quad (11)$$

Taking time derivative of Eq. 8 at  $t = 0$  yields,

$$\frac{\partial w}{\partial t} = \sum_{i=1}^{\infty} G_i X_i = \psi \quad \# \quad (12)$$

where  $\psi$  is velocity of the beam just after the impact as a function of  $x$ . By multiplying both sides of the above equation with  $X_j$ ,

$$\sum_{i=1}^{\infty} G_i X_i X_j = \psi X_j \quad \# \quad (13)$$

If Eq. 13 multiplied by  $m_2$  and evaluated at  $x = \frac{L}{2}$  is added to the integral of Eq. 13 with respect to the beam mass  $dm_1 = \left( \frac{m_1}{L} \right) dx$ , the following equation is obtained.

$$\sum_{i=1}^{\infty} G_i \left( \frac{2m_1}{L} \int_{x=0}^{\frac{L}{2}} X_i(x) X_j(x) dx + X_i\left(\frac{L}{2}\right) X_j\left(\frac{L}{2}\right) m_2 \right) = \frac{2m_1}{L} \int_{x=0}^{\frac{L}{2}} \psi(x) X_j(x) dx + \psi\left(\frac{L}{2}\right) X_j\left(\frac{L}{2}\right) m_2 \quad \# \quad (14)$$

Integration at left hand side of above equation vanishes when  $i \neq j$  which yields  $G_i$  as,

$$G_i = \frac{\frac{2m_1}{L} \int_{x=0}^{\frac{L}{2}} X_i \psi(x) dx + m_2 X_i\left(\frac{L}{2}\right) \psi\left(\frac{L}{2}\right)}{\frac{2m_1}{L} \int_{x=0}^{\frac{L}{2}} X_i^2 dx + m_2 X_i^2\left(\frac{L}{2}\right)} \quad \# \quad (15)$$

As assumed earlier that the impactor transfers its velocity entirely to the infinitesimal part of the beam at the contact point, we may write  $\frac{\partial w}{\partial t} = 0$  for  $t = 0, x \neq \frac{L}{2}$  and  $\frac{\partial w}{\partial t} = v_2$  for  $t = 0, x = \frac{L}{2}$  and  $G_i$  becomes

$$G_i = \frac{m_2 X_i\left(\frac{L}{2}\right) v_2}{\frac{2m_1}{L} \int_{x=0}^{\frac{L}{2}} X_i^2 dx + m_2 X_i^2\left(\frac{L}{2}\right)} = \frac{4v_2}{\phi_i \left( \frac{1}{\cos^2 \phi_i} - \frac{1}{\cosh^2 \phi_i} \right) + \frac{2m_1}{\phi_i m_2}} \quad \# \quad (16)$$

By writing the above equation in Eq. 8 the approximate beam displacement function can be written as follows,

$$w = \frac{L^2 v_2}{a^2} \sum_{i=1}^{\infty} \frac{1}{\phi_i^3} \frac{\frac{\sin^2 \phi_i x}{\cos \phi_i} - \frac{\sinh^2 \phi_i x}{\cosh \phi_i}}{\frac{1}{\cos^2 \phi_i} - \frac{1}{\cosh^2 \phi_i} + \frac{2m_1}{\phi_i^2 m_2}} \sin \frac{4\phi_i^2 a^2 t}{L^2} \quad \# \quad (17)$$

It should be noted that this approximate analytical solution is based on the classical beam theory and neglects the rotational inertia and shear effects.

### 2.1. The Finite Element Analysis

The following beam geometry and material properties were used to compare the displacements in transverse direction obtained from the analytical solution and finite element model. The beam has a square cross section with the dimensions of 0.01m x 0.01m, and its length is 0.4 m. Mass of the beam is  $m_1 = 0.314$  kg. The beam and striking sphere have the same material properties such that the density is  $7850 \text{ kg/m}^3$ , the modulus of elasticity is 200 GPa and Poisson's ratio is 0.3. Analysis were carried out for different striker sizes. The velocity of the striker just before the impact is  $v_2 = 4.63$  m/s downward for each case.

Models used in the finite element analysis were created in ABAQUS/Explicit software. Using the symmetry, a quarter geometry was modeled as shown in Fig. 2. Roller support condition was created on the bottom left edge of the beam along z-axis. The symmetry boundary conditions were applied on two vertical mid-sections of the beam and the sphere. The sphere was constrained to strike at the midspan and to move along transverse direction (y-direction) during the impact.

The finite element used in the analysis is C3D8R, which is a linear brick element with reduced integration. This finite element, unlike C3D8, has one integration point and eliminates the possibility of occurrence of locking. The shear locking is a problem for which there exists the formation of shear stresses that should not normally occur, and the elements tend to be too stiff under bending. Similarly, for the volume locking the finite elements behave too stiff during the incompressible or almost incompressible material behavior [18].

General contact algorithm with defaults was used for defining the interaction between beam and sphere. Beam and striking sphere were meshed with the same type of elements. Contact interaction property along the normal direction was hard contact allowing separation after contact. Tangential behavior was implemented as rough friction formulation with no slip on the contacting surfaces.

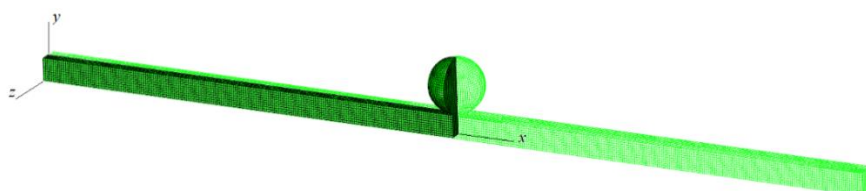


**Figure 2.** The geometry of quarter model for the beam and striker.

**Table 1.** The name of models used in the finite element analysis and their properties.

Model	R-50	R-75	R-100	R-125	R-150	R-175	R-200	R-300	R-400
Radius of striker (mm)	5	7.5	10	12.5	15	17.5	20	30	40
Mass ratio, $M (m_1/m_2)$	76.394	22.635	9.5493	4.8892	2.8294	1.7818	1.1937	0.3537	0.1492

A number of models with different mass ratios were considered, as given in Table 1. The beam dimensions were held constant while changing the radius of striker between the models. These models are shown in Fig. 3. An explicit dynamic analysis was performed in the solution. Time integration with explicit central finite differences can be performed effectively using small time increments. The finite elements solution has been obtained for a period of 16 ms starting from the initial contact which is sufficient to observe the vibrations and the sub-impacts.

Numerical calculations were carried out on a computer with 128GB of ram and 2.2 GHz 32 cores 64 threads dual CPU.

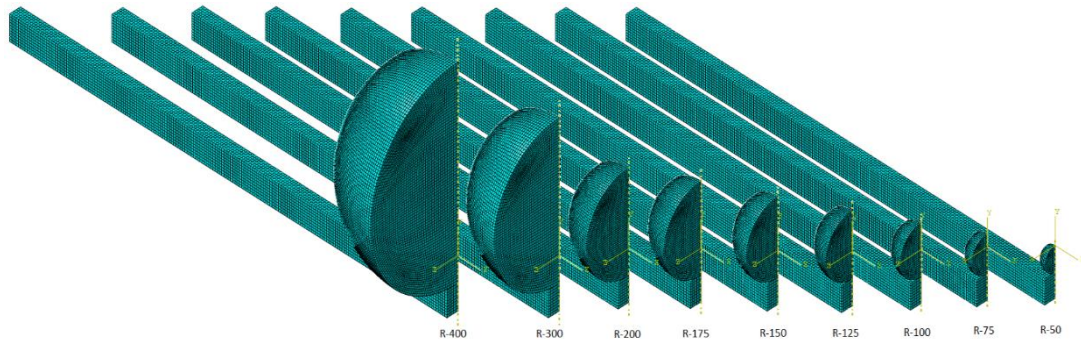


**Figure 3.** Models considered for the transverse impact between simply supported beam and sphere.

### 2.2. Mesh Size Analysis

A number of mesh distributions with different element sizes were considered. These mesh distributions are shown in Fig. 4. For each mesh from (a) to (e) in Fig. 4, the smallest element size formed at the impact point is 1 mm, 0.8 mm, 0.5 mm, 0.5 mm and 0.2 mm, respectively. Most of these have uniform element distribution. However, having smaller elements in the mesh, which decreases the "stable time increment" value, with the increase in number of elements prolongs the solution time significantly. Therefore, in order to reduce run time as much as possible, a non-uniform distribution was used for mesh (e). Total number of elements for each mesh is shown in Table 2. The CPU times of the solution range from 100 seconds to 9 hours.

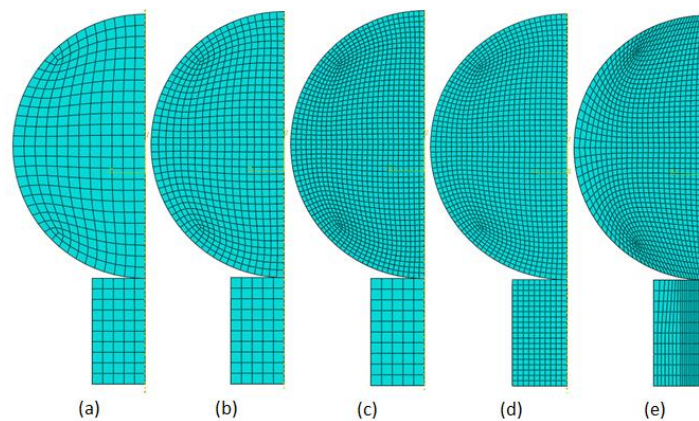


**Figure 4.** The finite element mesh distributions used for mesh size analysis.

In order to see the effect of element size on the solution, initially, the displacements obtained during the first contact were examined on the model R-125. The initial contact occurs within approximately 0.3 ms. As seen in Fig. 5 (a), the meshes from (a) to (d), present an element penetration occurred at certain amount. The sphere displacements indicated with the dashed lines are below the beam

displacements indicated with a solid line, these are the regions where the sphere and beam elements are penetrated at the contact point. Maximum penetration occurred for mesh (a) among these mesh types and this penetration is 0.024 mm occurred at 0.03 ms. During the initial contact, it is observed that element penetration at the contact point is quite small for mesh (e) as shown in Fig. 5 (b) which is 0.002 mm occurred at 0.03 ms.

**Table 2.** Total number of elements for each mesh.

Radius (mm)	Mesh (a)	Mesh (b)	Mesh (c)	Mesh (d)	Mesh (e)
5	10224	10550	11792	81792	12082
7.5	10744	11792	16048	86048	13434
10	13480	14466	25040	95040	22602
12.5	13480	20192	39120	109120	37090
15	16048	22750	60016	130016	37262
17.5	23568	28496	89072	159072	52228
20	30376	39120	127632	197632	128082
30	60016	109720	389948	459948	390450
40	127632	238640	914932	984932	915222

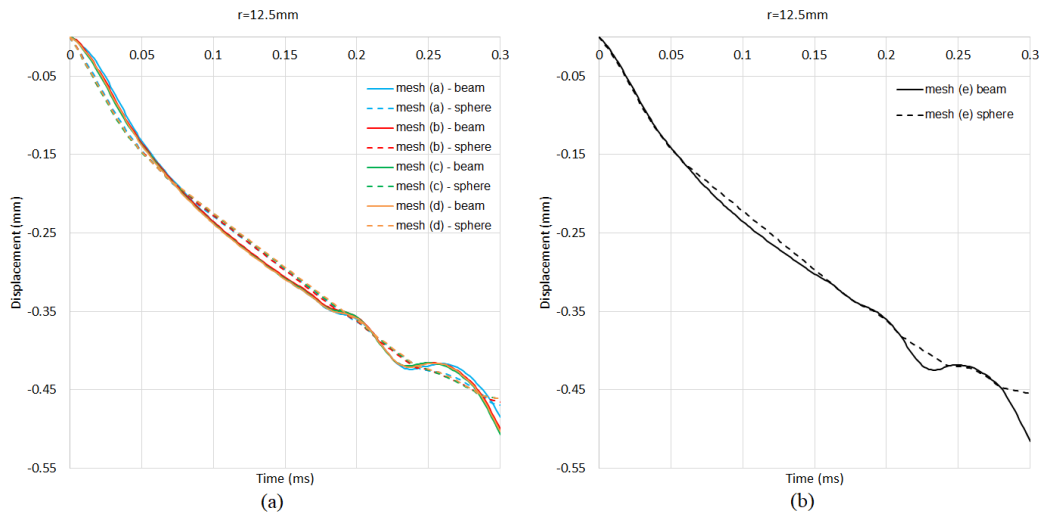


**Figure 5.** Displacements of the beam and striker during initial contact.

The beam deflections at the impact point and sphere displacements obtained from these meshes after the first contact are shown in Fig. 6. For the models without sub-impacts such as R-50 and R-75, the change in mesh size does not have a significant effect on the displacements of the impact point. For

other models, deflections obtained from each mesh are quite similar until the sub-impact. After the sub-impact, an apparent difference is observed in the beam deflections depending on the time of occurrence of the sub-impact between beam and sphere. During the initial contact the mesh size has a slight effect on the contact penetration and the displacements but small changes create a considerable effect on the velocity of the sphere and the time of occurrence of the sub-impact.

### **2.3. Verification with the Experimental Study**

In order to check the validity of the finite element model, a comparison was made with the results of the experimental study of Qi and Yin [29]. The geometric and mechanical properties used for the beam discussed in this section are the same as those used in the experimental study. As in the other numerical analyzes used in this study, the support conditions were chosen as simply supported and numerical analysis was performed using the quarter model. The finite element mesh used in numerical analysis is the mesh specified as mesh (e). Deflections for this problem are also computed using the analytical method and shown in Fig. 7.

The beam has the dimensions of  $b \times h = 60 \times 27.8 \text{ mm}^2$  and length of 780 mm. The density of the beam material is  $7800 \text{ kg/m}^3$ , the modulus of elasticity is 206 GPa and Poisson's ratio is 0.3. Mass of the beam is 10.213 kg. The striking sphere of 35 mm radius has a material density of  $7800 \text{ kg/m}^3$ , the modulus of elasticity is 208 GPa and Poisson's ratio is 0.33. Mass of the striker is 1.4008 kg. The mass ratio  $M$  is 7.29.

When the results of the finite element analysis are examined it is seen that the finite element model gives quite similar displacement values for the first two peaks in the displacement-time curve, although there were differences in the contact times of the sphere with the beam as shown in Fig. 7 (a). If the time-displacement graphs of the experimental study are examined, the damping of the beam displacements is clearly observed. At this point, it is possible to obtain results closer to the experimental results by introducing the damping in the finite element model. Accordingly, damping has been defined and the displacement values obtained are shown in Fig. 7 (b).

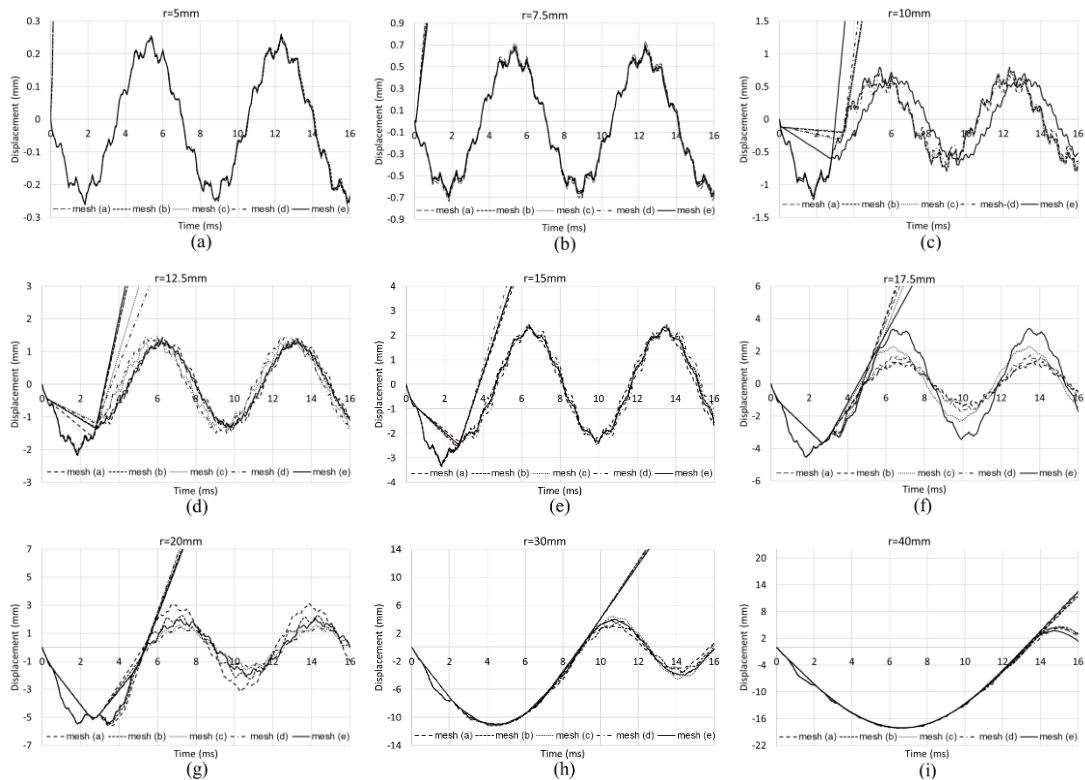


**Figure 6.** Displacements obtained by the mesh size analysis a)  $r=5\text{mm}$ , b)  $r=7.5\text{mm}$ , c)  $r=10\text{mm}$ , d)  $r=12.5\text{mm}$ , e)  $r=15\text{mm}$ , f)  $r=17.5\text{mm}$ , g)  $r=20\text{mm}$ , h)  $r=30\text{mm}$ , i)  $r=40\text{mm}$ .

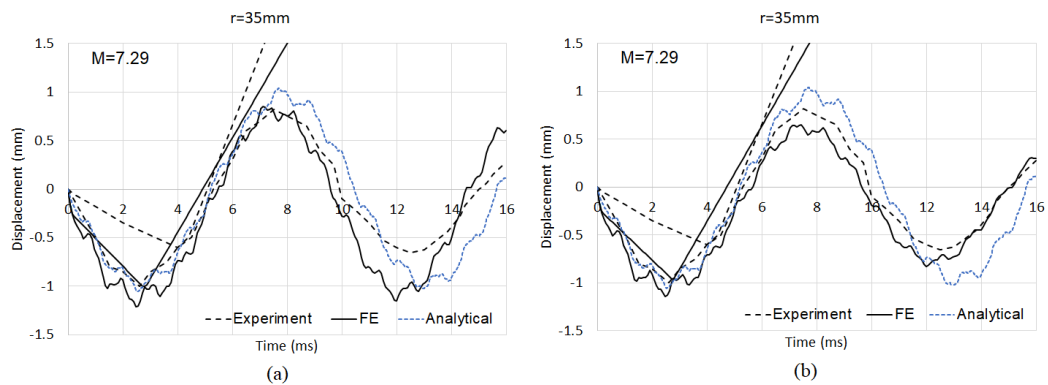


**Figure 7.** Displacements of the beam and striker a) without damping, b) with damping.

#### 2.4. Comparison Between the Analytical Solution and Finite Elements

First seven terms of the series in Eq. 17 were used to determine the deflections of the beam at contact point in the analytical solution. The  $\phi_i$  terms obtained from solution of the Eq. 9 are given in Table 3. In the finite element solution, smallest element sized mesh (e) was used. Comparison of the displacements are shown in Fig. 8.

Period of motion, as the duration between two crests in displacement – time graphs, observed for the analytical and finite element solutions are quite similar in the model with largest mass ratio, but there exists a difference in vibration amplitudes. In models where sub-impact occurs, it is observed that the analytical solution and finite element solution are quite compatible until the sub-impact. The maximum amplitude value after the sub-impact is smaller in finite element solution compared to analytical solution. In models where the mass ratio is very small and the radius of the impacting sphere is large, sub-impacts turn into continuous contact and deflections obtained from the analytical solution and the finite element solution during this stage are very close. For these models as well, after the contact ends, there exists a difference between the amplitude values calculated in the analytical solution and in the finite element solution. The analytical and finite element solutions are more compatible during the time when sphere and beam are in contact.

**Table 3.** The values of  $\phi_i$  based on mass ratio.

Radius of striker (mm)	Mass of striker (kg)	$\frac{m_1}{m_2}$ ratio	$\phi_1$	$\phi_2$	$\phi_3$	$\phi_4$	$\phi_5$	$\phi_6$	$\phi_7$
5	0.00411	76.394	1.5606	4.6827	7.8054	10.929	14.053	17.178	20.304
7.5	0.01387	22.635	1.5379	4.6201	7.7095	10.805	13.906	17.012	20.122
9	0.02397	13.099	1.5159	4.5651	7.6321	10.713	13.805	16.905	20.012
9.35	0.02688	11.6825	1.5098	4.5508	7.6130	10.691	13.782	16.882	19.988
9.6	0.02909	10.7934	1.5053	4.5403	7.5993	10.676	13.766	16.865	19.972
10	0.03288	9.5493	1.4977	4.5232	7.5772	10.652	13.741	16.840	19.948
12.5	0.06422	4.8892	1.4413	4.4110	7.4460	10.517	13.610	16.716	19.830
15	0.1110	2.8294	1.3734	4.3045	7.3400	10.421	13.521	16.638	19.760
17.5	0.1762	1.7818	1.3000	4.2157	7.2631	10.356	13.468	16.590	19.718
20	0.2631	1.1937	1.2264	4.1468	7.2097	10.314	13.433	16.560	19.692
30	0.8878	0.3537	0.9754	4.0076	7.1159	10.244	13.378	16.514	19.653
40	2.104	0.1492	0.8038	3.9629	7.0892	10.224	13.363	16.502	19.643

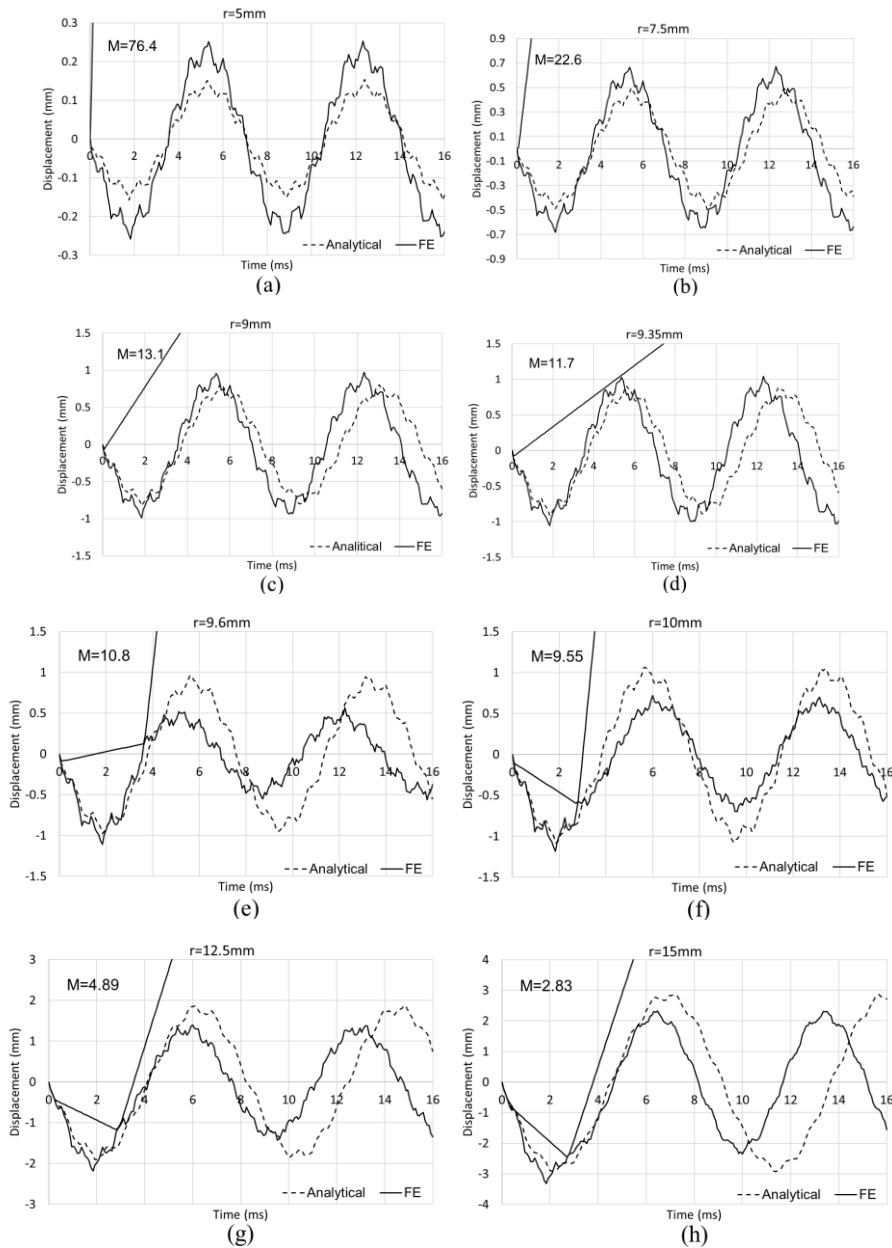


**Figure 8.** Displacements obtained from analytical solution and finite element solution a)  $M=76.4$  b)  $M=22.6$ , c)  $M=13.1$ , d)  $M=11.7$ , e)  $M=10.8$ , f)  $M=9.55$ , g)  $M=4.89$ , h)  $M=2.83$ , i)  $M=1.78$ , j)  $M=1.19$ , k)  $M=0.35$ , l)  $M=0.15$ .

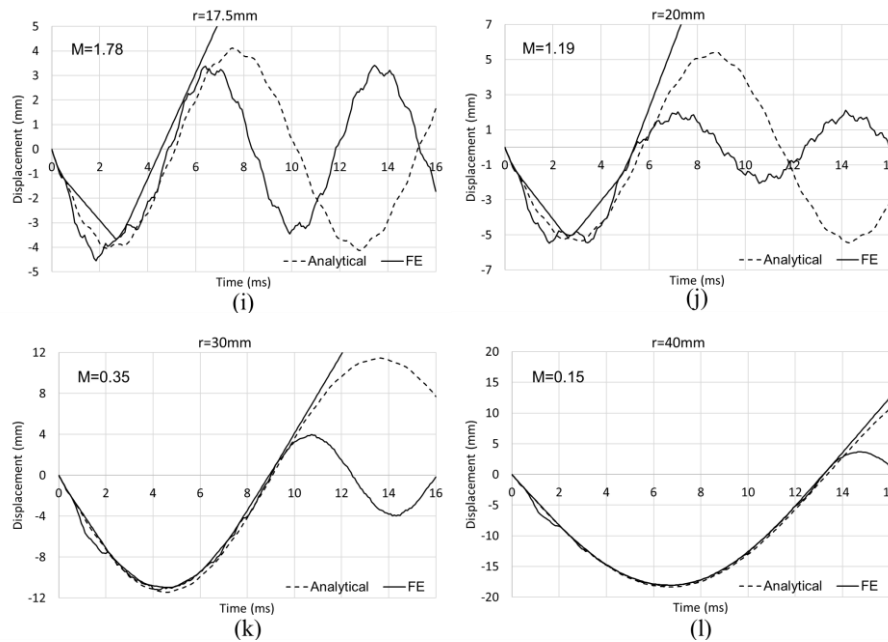


**Figure 8.** (Cont.) Displacements obtained from analytical solution and finite element solution a)  $M=76.4$  b)  $M=22.6$ , c)  $M=13.1$ , d)  $M=11.7$ , e)  $M=10.8$ , f)  $M=9.55$ , g)  $M=4.89$ , h)  $M=2.83$ , i)  $M=1.78$ , j)  $M=1.19$ , k)  $M=0.35$ , l)  $M=0.15$ .

### 2.5. Effect of Sub-impact

If the impacting sphere is small, the period of interaction is very small instant of time which results in a direct separation of beam and sphere. In case of large mass impact onto a slender beam, there exists substantial structural deformations and energy loss to structural vibrations [33]. As the mass ratio decreases, the velocity of the sphere after the initial contact decreases. This results in secondary contacts that occur as the beam continues its motion. From the finite element analysis, it has been observed that sub-impacts occur when the mass ratio is less than 11.6 as shown in Fig. 9. As the mass ratio approaches to 1 the number of sub-impacts increases as shown in Fig. 8 (i) and Fig. 8 (j). As the ratio decreases further repetitive contacts give way to a state of continuous contact as shown in Fig. 8 (k) and Fig. 8 (l) until the sphere leaves the beam.

If a case is created by forcing the sphere to move upward, a finite element analysis can be done without the effect of sub-impacts on the beam motion. This forcing was realized by applying an artificial upward displacement on the sphere after the first contact. The deflection of the impact point on the beam obtained from this analysis is shown in Fig. 10 with dashed lines for a sphere of 10 mm radius and a mass ratio of  $M = 9.55$ . In this case, the amplitude value is 1.16 mm. In the actual case, the displacement amplitude after the sub-impact is 0.72 mm. This corresponds to a 38% reduction in

the amplitude. Sub-impact causes the point on the beam to displace less and the subsequent amplitude values to continue at

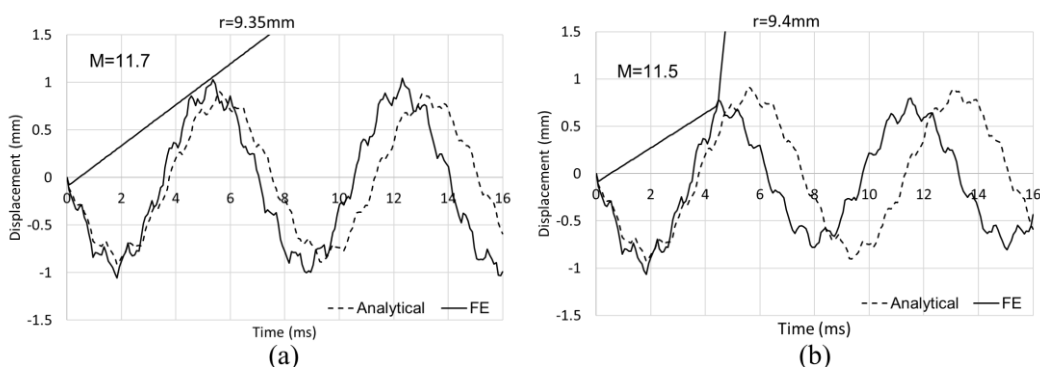


**Figure 9.** Displacements a) without sub-impact and b) with sub-impact.

this level. Furthermore, period of motion is around 7 ms for both cases. This value is quite close to the natural period,  $T_n$ , for the first free vibration mode of a simply supported beam when the mass is spread uniformly over its length. If one calculate the natural period using  $T_n = \frac{2}{\pi} \sqrt{\frac{qL^4}{EI}}$  where  $q$  is mass per unit length [25],  $T_n = 7ms$ . The period value occurred around 7 ms in all finite element solutions.

The graph in Fig. 11 (a) shows variation of the maximum deflection of impact point on the beam after the initial contact, with the mass ratio,  $M$ . The analytical and finite element solutions yield similar maximum deflection values for the values of  $M$  close to 1 or less than 1. In this case, relatively large mass creates a single loading-unloading mechanism as mentioned in [34]. Maximum difference between the deflections obtained from the analytical and finite element solution is 39% which is observed for the largest mass ratio, that is for the smallest impactor mass. The analytical solution underestimates the deflection with respect to finite element solution for small sphere mass. It should be noted that the approximate displacement function is based on Euler-Bernoulli beam theory and it does not consider the actual contact force in the vibration equation. On the other hand, the finite element model is based on a 3d continuum element which does not have the assumptions of Euler-Bernoulli beam theory. Fig. 11 (b) shows the maximum upward deflection of the beam, i.e. the amplitude at the crest of the vibration, and reduction percent of the amplitude because of the sub-impact. The dashed line in the graph indicates the finite element results when the occurrence of sub-impacts is restricted.

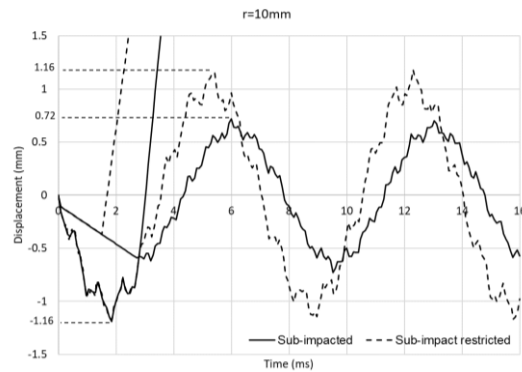


**Figure 10.** Decrease in the amplitude due to the sub-impact.

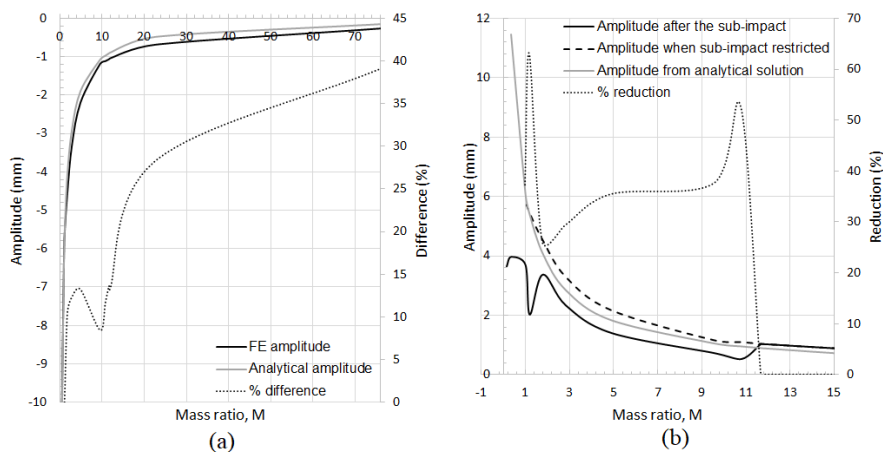


**Figure 11.** The maximum deflection of impact point (a), the amplitude at the crest of the vibration (b).

### 3. CONCLUSIONS

In this study, a comparison between the analytical solution and finite element solution was made for the transverse impact problem of a sphere to a simply supported beam. The deflection equation, given by Goldsmith [4], of an elastic beam impacted by a rigid sphere was considered in the analytical solution. Finite element solutions were obtained in ABAQUS for a number of models with different mass ratios and various mesh sizes. Deflections of the beam and displacement of the sphere were calculated at the contact point.

A mesh size analysis was carried out first with various mesh sizes. The deflections of the beam and the sub-impact effects were investigated. First seven term of the series were used in the analytical

solution and the smallest element sized mesh was used in the finite element solutions. According to this;

1. Through the mesh size analysis, in models without sub-impacts such as R-50 and R-75 it is observed that, change in the mesh size has no significant effect on the calculated value of the beam deflection. For models with sub-impacts, the mesh size has also no significant effect on the beam deflections until the start of sub-impacts. Change in the mesh size results a slight change in the occurrence time of the sub-impacts. Therefore, amplitude of the vibration obtained from each mesh at the impact point also changes after the sub-impact process.
2. In the model with the largest mass ratio, the analytical solution and finite element solution yield similar vibration periods, but analytical solution underestimates the maximum deflection with respect to the finite element solution.
3. In models with sub-impacts, it is observed that the analytical solution and finite element solution are quite compatible until the sub-impact occurs. However, the finite element solution gives smaller amplitude values compared to the analytical solution after the sub-impact.
4. The sub-impacts are observed for the mass ratio less than a certain value. This value is  $M=11.6$  for the models considered in this study.
5. In models with small mass ratio, sub-impacts turn into continuous contact and during this time period the analytical solution and the finite element solution are in very close agreement. After the contact period ends, a difference has arisen between the analytical solution and the finite element solution for the amplitude values calculated in these models.
6. As the mass ratio decreases, the maximum deflection value becomes more compatible for the analytical solution and the finite element solution. Maximum difference is 39% and the difference is less than 13% for the mass ratio values smaller than  $M=11.6$ .
7. As the mass ratio changes, the period of vibration obtained from the analytical solution changes, whereas the period of vibration remains the same in the finite element solution. For the largest mass ratio, the vibration period obtained from analytical solution and the finite element solution are quite close, but as the mass ratio decreases analytical solution gives larger vibration period values compared to finite element solution.

Because the impactor and beam are assumed to remain in contact, the analytical solution does not provide any information about the motion of impactor, the sub-impacts and effect of sub-impacts on displacements. Despite the assumptions made, this method yields maximum deflection values that correlate well with the finite elements especially for small mass ratio, i.e. for large-mass impact onto the beam. As the mass ratio decreases, bending becomes more significant and it prolongs the period of contact. For cases of large mass ratio,  $M$ , the period of interaction is very small instant of time so that the contact force has a very short range. Small mass impact is worth further studying. A solution including forcing function  $F$  can produce better results especially for small-mass impact.

#### **ACKNOWLEDGMENT**

The authors received no specific grant for the research, authorship, and/or publication of this article.

## REFERENCES

- [1] Cox, H., (1849), On impacts on elastic beams, Cambridge Philosophical Transactions, 9, 73-78.
- [2] Timoshenko, S.P., (1913), Zur frage nach der wirkung eines stosses auf einen balken, Zeitschrift für Mathematik und Physik, 62(2), 198-209.
- [3] Hertz, H., (1881), Über die berührung fester elastischer körper, Journal für die Reine und Angewandte Mathematik, 92, 156-171.
- [4] Goldsmith, W., (2001), Impact the theory and physical behaviour of colliding solids, Dover Publications, New York.
- [5] Gültop, T., Yılmaz, M.C., Alyavuz, B., (2015), An analytical investigation of rigid plastic beams under impact loading, Journal of the Faculty of Engineering and Architecture of Gazi University, 30(1), 87-94.
- [6] Eringen, A.C., (1952), Transverse impact on beams and plates with arbitrary edge conditions, Naval Research Department Technical Report No 2.
- [7] Schwieger, H., (1965), A simple calculation of the transverse impact on beams and its experimental verification, Experimental Mechanics, 5(11), 378-384.
- [8] Yılmaz, M.C., Anıl, Ö., Alyavuz, B., Kantar, E., (2014), Load displacement behavior of concrete beam under monotonic static and low velocity impact load, International Journal of Civil Engineering Transaction A: Civil Engineering, 12(4), 88-503.
- [9] Anıl, Ö., Kantar, E., Yılmaz, M.C., (2015), Low velocity impact behavior of rc slabs with different support types, Construction and Building Materials, 93, 1078-1088.
- [10] Jin, L., Xu, J., Zhang, R., Du, X., (2017), Numerical study on the impact performances of reinforced concrete beams: a mesoscopic simulation method, Engineering Failure Analysis, 80, 141-163.
- [11] Othman, H., Marzouk, H., (2017), Finite-element analysis of reinforced concrete plates subjected to repeated impact loads, Journal of Structural Engineering, 143(9), 04017120.
- [12] Saatci, S., Vecchio, F.J., (2009), Nonlinear finite element modeling of reinforced concrete structures under impact loads, ACI Structural Journal, 106(5), 717-725.
- [13] Qiao, P., Yang, M., (2007), Impact analysis of fiber reinforced polymer honeycomb composite sandwich beams, Composites Part B: Engineering, 38(5-6), 739-750.

- [14] Foo, C.C., Seah, L.K., Chai, G.B., (2008), Low-velocity impact failure of aluminum honeycomb sandwich panels, *Composite Structures*, 85(1), 20-28.
- [15] Hughes, T.J., Taylor, R.L., Sackman, J.L., (1975), Finite element formulation and solution of contact-impact problems in continuum mechanics-IV Report No. UC SESM 76-4, Department of Civil Engineering University of California, Berkeley.
- [16] Hughes, T.J.R., Taylor, R.L., Sackman, J.L., Curnier, A., Kanoknukulchai, W., (1976), A finite element method for a class of contact-impact problems, *Computer Methods in Applied Mechanics and Engineering*, 8(3), 249-276.
- [17] [Belytschko, T., Liu, W.K., Moran, B., (2000), *Nonlinear finite elements for continua and structures*, Wiley, Chichester.
- [18] ABAQUS Analysis User's Manual, (2011), Simulia.
- [19] Yu, J., Jones, N., (1989), Numerical simulation of a clamped beam under impact loading, *Computers and Structures*, 32(2), 281-293.
- [20] Yu, J., Jones, N., (1997), Numerical simulation of impact loaded steel beams and the failure criteria, *International Journal of Solids and Structures*, 34(30), 3977-4004.
- [21] Li, Q.M., Jones, N., (2002), Response and failure of a double-shear beam subjected to mass impact, *International Journal of Solids and Structures*, 39(7), 1919-1947.
- [22] Al-Thairy, H., Wang, Y.C., (2011), A numerical study of the behaviour and failure modes of axially compressed steel columns subjected to transverse impact, *International Journal of Impact Engineering*, 38(8-9), 732-744.
- [23] Wang, R., Pei, C., (2013), Parametric analysis of dynamic response of hot-rolled h-shaped steel beam under lateral impact load, *Gongcheng Lixue/Engineering Mechanics*, 30(SUPPL.1), 258-262.
- [24] Shi, S., Zhu, L., Yu, T.X., (2019), Dynamic modelling of elastic-plastic beams under impact, *International Journal of Impact Engineering*, 126, 1-10.
- [25] Pashah, S., Massenzio, M., Jacquelin, E., (2008), Prediction of structural response for low velocity impact, *International Journal of Impact Engineering*, 35(2), 119-132.
- [26] Zhang, L., Yin, X., Yang, J., Wang, H., Deng, Q., Yu, B. et al, (2018), Transient impact response analysis of an elastic-plastic beam, *Applied Mathematical Modelling*, 55, 616-636.
- [27] Seifried, R., (2006), Multiple impacts of transversely struck aluminum beams, *Proceedings in Applied Mathematics & Mechanics*, 6, 333-334.

- [28] Arnold, R.N., (1937), Impact stresses in a freely supported beam, Proceedings of the Institution of Mechanical Engineers, 137(1), 217-281.
- [29] Qi, X., Yin, X., (2016), Experimental studying multi-impact phenomena exhibited during the collision of a sphere onto a steel beam, Advances in Mechanical Engineering, 8(9), 1-16.
- [30] LS-DYNA Theory Manual, (2006), Livermore Software Technology Corporation, Livermore.
- [31] Qi, X., Yin, X., (2017), Sub-impacts of simply supported beam struck by steel sphere - Part II: Numerical simulations, Advances in Mechanical Engineering, 9(1), 1-11.
- [32] Weaver, W., Timoshenko, S.P., Yong, D.H., (1990), Vibration problems in engineering, John Wiley & Sons, New York.
- [33] Stronge, W. J., (2000), Impact mechanics, Cambridge University Press, Cambridge.
- [34] Olsson, R., (2015), Analytical prediction of damage due to large mass impact on thin ply composites, Composites: Part A, 72, 184-191.